

# The WKB Local Discontinuous Galerkin Method for the Simulation of Schrödinger Equation in a Resonant Tunneling Diode

Wei Wang · Chi-Wang Shu

Received: 2 February 2008 / Revised: 31 July 2008 / Accepted: 1 August 2008  
© Springer Science+Business Media, LLC 2008

**Abstract** In this paper, we develop a multiscale local discontinuous Galerkin (LDG) method to simulate the one-dimensional stationary Schrödinger-Poisson problem. The stationary Schrödinger equation is discretized by the WKB local discontinuous Galerkin (WKB-LDG) method, and the Poisson potential equation is discretized by the minimal dissipation LDG (MD-LDG) method. The WKB-LDG method we propose provides a significant reduction of both the computational cost and memory in solving the Schrödinger equation. Compared with traditional continuous finite element Galerkin methodology, the WKB-LDG method has the advantages of the DG methods including their flexibility in  $h$ - $p$  adaptivity and allowance of complete discontinuity at element interfaces. Although not addressed in this paper, a major advantage of the WKB-LDG method is its feasibility for two-dimensional devices.

**Keywords** Local discontinuous Galerkin method · WKB-LDG method · Schrödinger equation · Resonant tunneling diode

## 1 Introduction

In recent studies of nanoscale semiconductor structures, quantum effects arise and have to be taken into account in the modeling by means of the Schrödinger equation. There are computational difficulties in solving the Schrödinger equations. On the one hand, the oscillatory

---

Research supported by NSF grants DMS-0510345 and DMS-0809086.

W. Wang (✉) · C.-W. Shu  
Division of Applied Mathematics, Brown University, Providence, RI 02912, USA  
e-mail: [wwang@dam.brown.edu](mailto:wwang@dam.brown.edu)

C.-W. Shu  
e-mail: [shu@dam.brown.edu](mailto:shu@dam.brown.edu)

*Present address:*

W. Wang  
Center for Turbulence Research, Stanford University, Stanford, CA 94305, USA  
e-mail: [weiwang1@stanford.edu](mailto:weiwang1@stanford.edu)

behavior of the solutions requires a refined spacial grid. On the other hand, a large number of Schrödinger equations need to be solved in order to simulate an electronic device. For example, in the resonant tunneling diode (RTD) [4, 5, 16], only the electrons having an energy extremely close to the resonant energy are transmitted from the source to the drain. To collect the resonances, there are thousands of Schrödinger equations to solve.

In [4], Ben Abdallah and Pinaud proposed a WKB approach using traditional continuous finite element method for a one dimensional model. They obtained an explicit formula for the phase factor of wave functions from WKB asymptotics [6] and then used this phase factor to interpolate the nodal values of the wave function. Therefore, a much coarser grid is allowed compared with the method based on polynomials. A convergence analysis for this method is presented in [14]. In [3], this method is generalized to a special two dimensional device in which the two dimensional Schrödinger equation is approximated by a one dimensional non-diagonal Schrödinger system [17] for which a WKB type approach can be derived (see [15]). One limitation of the method in these works is, however, that it is difficult to be generalized to general two-dimensional devices for which the two dimensional Schrödinger equation cannot be easily converted to one dimensional systems and must be solved in two dimensional elements, as it is very difficult to have continuity at the element interface with such multiscale basis functions in two dimensions.

Compared with traditional continuous finite element Galerkin methodology, the advantage of the discontinuous Galerkin (DG) and the local DG (LDG) methods includes their flexibility in  $h$ - $p$  adaptivity and their allowance of complete discontinuity at element interfaces. Stable and convergent LDG methods have been designed for elliptic equations in [1, 9]. A multiscale DG method based on non-polynomial approximation spaces has been developed in [18, 19]. We also refer the reader to [10] for a review of the DG methods. It is computationally advantageous to combine the WKB approach with the LDG method, which is the main purpose of this paper: we present a WKB-LDG method to solve the Schrödinger equation, which is in essence an LDG method based on exponential basis functions in the spirit of [18]. The method maintains the advantages of the general DG/LDG methods and saves in computational cost as well as memory when compared with the regular polynomial-based LDG methods. To conveniently compare our results to those obtained with the traditional continuous finite element WKB method, we take mostly the same examples as in [4]. The results in this paper are only one-dimensional, however it is feasible to extend the WKB-LDG method to two-dimensional devices, because there is no continuity requirement for the solution across element interfaces. The extension to two-dimensional devices does involve the non-trivial task of constructing suitable multiscale basis functions, which involves an accurate estimate of the local oscillation direction and is left for future work. We remark that, in recent years, there have been many contributions in developing DG methods for solving PDEs in semi-conductor device simulations, such as those in [7, 8, 12, 13]. Compared with these earlier works, our work is the first time of using the DG method to solve the RTD model with Schrödinger equation and also the first time to apply exponential approximation spaces in the DG method for solving the Schrödinger equation.

### 1.1 The Schrödinger-Poisson Problem

The RTD model (see [4]) extends on the interval  $[a, b]$  with  $a < a_1 < a_2 < a_3 < b_3 < b_2 < b_1 < b$  along the growth direction  $x$ . Its conduction band profile consists of two barriers of height  $v_1$  located at  $[a_2, a_3]$  and  $[b_3, b_2]$ . A bias energy  $\Delta v$  is applied between the source ( $x < a_1$ ) and the collector ( $x > b_1$ ) regions. The regions  $[a, a_1]$  and  $[b_1, b]$  are highly doped with doping density  $n_d^1$ , and  $[a_1, a_2]$  and  $[b_2, b_1]$  are doped with  $n_d^2$ . The transport is assumed

to be ballistic and one-dimensional. The wave function of the electrons injected at  $x = a$  with momentum  $p \geq 0$  satisfies a stationary effective-mass Schrödinger equation with open boundary conditions [2]:

$$\begin{cases} -\frac{\hbar^2}{2m}\varphi_p'' - qV\varphi_p = E_p^a\varphi_p, & (p \geq 0), \\ \hbar\varphi_p'(a) + ip\varphi_p(a) = 2ip; & \hbar\varphi_p'(b) = ip_b\varphi_p(b), \end{cases} \tag{1.1}$$

where  $\hbar$  is the reduced Plank constant,  $m$  is the effective mass (assumed to be constant in the device),  $q$  is the elementary positive charge of the electron,  $V$  is the total electrostatic potential in the device and

$$p_b = \sqrt{p^2 + 2qm(V_b - V_a)}, \quad E_p^a = \frac{p^2}{2m} - qV_a$$

with  $V_a$  and  $V_b$  being the given constant electrostatic potential at the source contact  $a$  and at the drain contact  $b$  respectively.

Similarly, the wave function of electrons injected at  $x = b$  with momentum  $p \leq 0$  satisfies the equation:

$$\begin{cases} -\frac{\hbar^2}{2m}\varphi_p'' - qV\varphi_p = E_p^b\varphi_p, & (p \leq 0), \\ \hbar\varphi_p'(b) + ip\varphi_p(b) = 2ip; & -\hbar\varphi_p'(a) = ip_a\varphi_p(a), \end{cases} \tag{1.2}$$

where

$$p_a = \sqrt{p^2 + 2qm(V_a - V_b)}, \quad E_p^b = \frac{p^2}{2m} - qV_b.$$

The transmission coefficients are defined by

$$T(p) = \frac{\sqrt{(p^2 + 2qm(V_b - V_a))^+}}{|p|} |\varphi_p(b)|^2 \quad \text{for } p \geq 0, \tag{1.3}$$

$$T(p) = \frac{\sqrt{(p^2 + 2qm(V_b - V_a))^+}}{|p|} |\varphi_p(a)|^2 \quad \text{for } p < 0, \tag{1.4}$$

where  $(a)^+ = \max(a, 0)$ .

The electrons are assumed to be in a mixed state so that the electronic density is given by

$$n(x) = \int_{-\infty}^{\infty} g(p) |\varphi_p(x)|^2 dp, \tag{1.5}$$

where  $g(p) := g_a(p)$  for  $p \geq 0$  and  $g(p) := g_b(p)$  for  $p < 0$ .  $g_a$  and  $g_b$  are the statistics of the electrons injected at  $x = a$  and  $x = b$  respectively. In our case,  $g(p)$  is a Fermi-Dirac integral given by

$$g(p) = \frac{mk_bT}{2\pi^2\hbar^3} \log \left( 1 + \exp \left( \left( -\frac{p^2}{2m} + E_F \right) / k_bT \right) \right), \tag{1.6}$$

where  $k_b$  is the Boltzmann constant and  $E_F$  is the Fermi energy defined implicitly by the neutrality condition for the doping density in the source and drain regions (see [5]):

$$n_d^1 = \int_{-\infty}^{\infty} g(p) dp. \tag{1.7}$$

The current density is given by

$$J = \frac{q}{m} \int_{-\infty}^{\infty} g(p) p T(p) dp. \tag{1.8}$$

The electrostatic potential  $V = V_e + V_s$ .  $V_e$  is the external potential including double barriers and applied bias and  $V_s$  is the self-consistent potential modeling the electron-electron interaction

$$\begin{cases} V_s''(x) = \frac{q}{\epsilon} (n(x) - n_D(x)), \\ V_s(a) = V_s(b) = 0, \end{cases} \tag{1.9}$$

where  $\epsilon$  is the dielectric constant and  $n_D$  is the doping density.

Since the equations (1.1), (1.2), (1.5) and (1.9) are coupled together, the Gummel method [11] is used to accelerate the iterating speed (see [16]). We solve

$$\frac{d^2 V_s^{new}}{dx^2} = \frac{q}{\epsilon} [n(V_s^{old}) \exp((V_s^{new} - V_s^{old})/V_{ref}) - n_D] \tag{1.10}$$

instead of (1.9), where the potential reference  $V_{ref}$  is adjusted to decrease the number of iterations. The linear version of the Gummel method is given by

$$\frac{d^2 V_s^{new}}{dx^2} = \frac{q}{\epsilon} \left[ n(V_s^{old}) \left( 1 + \frac{(V_s^{new} - V_s^{old})}{V_{ref}} \right) - n_D \right]. \tag{1.11}$$

When no bias is applied, the Gummel method converges with zero as an initial guess for the self-consistent potential. When the bias is not zero, the potential obtained from the no-bias case is used to initialize the algorithm.

### 1.2 The WKB Approach

In [4], the authors have presented a WKB scheme using the continuous finite element method. The motivation of their basis construction comes from the WKB asymptotics [6], i.e. for  $E + qV(x) > 0$  (where  $E$  is the given energy in the Schrödinger equation, i.e.  $E_p^a$  in (1.1) or  $E_p^b$  in (1.2)) and when  $\hbar \rightarrow 0$ ,

$$\varphi(x) \sim \frac{A}{\sqrt[4]{2m(E + qV(x))}} e^{iS(x)} + \frac{B}{\sqrt[4]{2m(E + qV(x))}} e^{-iS(x)}, \tag{1.12}$$

where  $A$  and  $B$  are constants,  $S(x)$  is the dimensionless action,

$$S(x) = \frac{\sqrt{2m}}{\hbar} \int_{x_0}^x \sqrt{E + qV(s)} ds \tag{1.13}$$

and  $x_0$  is an integration constant. Therefore, their WKB-interpolated function in the continuous finite element case for the cell  $I_j$  is given by

$$\tilde{\varphi}(x) = \frac{A_j}{\sqrt[4]{2m(E + qV(x))}} e^{iS(x)} + \frac{B_j}{\sqrt[4]{2m(E + qV(x))}} e^{-iS(x)}, \quad x \in I_j. \tag{1.14}$$

The constants  $A_j$  and  $B_j$  are determined by the nodal values at the cell boundaries.

We will introduce a similar idea but based on the LDG methodology, which is called the WKB-LDG method in next section.

## 2 Numerical Methods

In this section, we are going to first introduce the regular LDG solver for the Schrödinger equations and the minimal dissipation LDG (MD-LDG) solver [9] for the Poisson potential equation (1.9). Then we define the WKB-LDG method for (1.1) and (1.2). For more details of the LDG methods for elliptic equations, including stability analysis and error estimates, we refer to [1].

### 2.1 Traditional LDG Methods for the Schrödinger Equations

For simplicity, we first write the stationary Schrödinger equation (1.1) as follows

$$\begin{cases} -\varphi_p'' - a(x)\varphi_p = 0, & (p \geq 0), \\ \hbar\varphi_p'(a) + ip\varphi_p(a) = 2ip; \quad \hbar\varphi_p'(b) = ip_b\varphi_p(b), \end{cases} \tag{2.1}$$

where

$$a(x) = \frac{2m}{\hbar^2}(qV + E^q).$$

Since the equation is linear for given  $V$ , we can first solve for  $\tilde{\varphi}_p$  on a boundary condition  $\tilde{\varphi}_p(a) = 1$  and  $\tilde{\varphi}_p'(b) = \frac{ip_b}{\hbar}\tilde{\varphi}_p(b)$  and then normalize  $\tilde{\varphi}_p$  by  $2ip/[\hbar\tilde{\varphi}_p'(a) + ip\tilde{\varphi}_p(a)]$  to recover  $\varphi_p$  (see [16]).

Therefore, we apply the LDG method on the PDE

$$\begin{cases} -u'' - a(x)u = 0, \\ u(a) = 1; \quad u'(b) = c_b u(b), \end{cases} \tag{2.2}$$

where  $c_b = ip_b/\hbar$  is a constant for fixed  $p$ . Notice that we have used  $u$  to denote  $\tilde{\varphi}_p$ .

In order to define the LDG method, we rewrite the PDE (2.2) into a system of first order equations

$$q - u_x = 0, \quad -q_x - a(x)u = 0. \tag{2.3}$$

Let  $I_j = (x_{j-\frac{1}{2}}, x_{j+\frac{1}{2}})$ ,  $j = 1, \dots, N$ , be a partition of the computational domain,  $x_j = \frac{1}{2}(x_{j-\frac{1}{2}} + x_{j+\frac{1}{2}})$ ,  $\Delta x_j = x_{j+\frac{1}{2}} - x_{j-\frac{1}{2}}$  and  $h = \max_j \Delta x_j$ . The polynomial-based DG space is

$$V_h^k = \{v_h : (v_h)|_{I_j} \in P^k(I_j), \quad j = 1, \dots, N\} \tag{2.4}$$

where  $P^k(I_j)$  denotes the set of all polynomials of degree at most  $k$  in the interval  $I_j$ .

Note that in  $V_h^k$ , the functions are allowed to have jumps at the interfaces  $x_{j+\frac{1}{2}}$ . This is one of the main differences between the DG method and most other finite element methods. Moreover, both the mesh sizes  $\Delta x_j$  and the degree of polynomials  $k$  can be changed from element to element freely, thus allowing the  $h$ - $p$  adaptivity.

For a function  $v_h \in V_h^k$ , since it is discontinuous at the interface  $x_{j+\frac{1}{2}}$ , we use  $(v_h)_{j+\frac{1}{2}}^-$  and  $(v_h)_{j+\frac{1}{2}}^+$  to refer to the left and right limits of  $v_h$  at  $x_{j+\frac{1}{2}}$ , respectively.

The general formulation of the LDG method for the elliptic problem (2.2) is to find  $u_h, q_h \in V_h^k$  such that

$$\int_{I_j} q_h w_h dx + \int_{I_j} u_h (w_h)_x dx - \widehat{u}_{h,j+\frac{1}{2}} (w_h)_{j+\frac{1}{2}}^- + \widehat{u}_{h,j-\frac{1}{2}} (w_h)_{j-\frac{1}{2}}^+ = 0, \tag{2.5}$$

$$\int_{I_j} q_h(v_h)_x dx - \widehat{q}_{h,j+\frac{1}{2}}(v_h)_{j+\frac{1}{2}}^- + \widehat{q}_{h,j-\frac{1}{2}}(v_h)_{j-\frac{1}{2}}^+ - \int_{I_j} a(x)u_h v_h dx = 0 \tag{2.6}$$

for  $j = 1, 2, \dots, N$  and all test functions  $v_h, w_h \in V_h^k$ .

The numerical fluxes  $\widehat{u}_h$  and  $\widehat{q}_h$  are chosen to be the alternate fluxes:  $\widehat{u}_h = u_h^-$  and  $\widehat{q}_h = q_h^+$ . At the two boundary points,  $\widehat{u}_{h,\frac{1}{2}} = u(a)$  and  $\widehat{q}_{h,N+\frac{1}{2}} = c_b(u_h)_{N+\frac{1}{2}}^-$ . In this one-dimensional case, this LDG scheme is guaranteed to give an optimal convergence rate of  $h^{k+1}$  in  $L^2$  norm for both  $u$  and  $q$ .

Similarly, we can solve the Schrödinger equation with  $p < 0$ . We solve the following PDE for  $u$  first, then normalize it by  $2ip/[\hbar u'_p(b) + ipu_p(b)]$ :

$$\begin{cases} -u'' - a(x)u = 0, \\ u(b) = 1; \quad u'(a) = c_a u(a), \end{cases} \tag{2.7}$$

where  $c_a = -ip_a/\hbar$ . Since the boundary conditions are opposite to the  $p > 0$  case, the numerical fluxes should also be opposite, i.e. we take  $\widehat{u}_h = u_h^+$  and  $\widehat{q}_h = q_h^-$ . At the two boundary points,  $\widehat{u}_{h,N+\frac{1}{2}} = u(b)$  and  $\widehat{q}_{h,\frac{1}{2}} = c_a(u_h)_{\frac{1}{2}}^+$ .

### 2.2 The MD-LDG Method for the Poisson Potential Equation

We use the MD-LDG method to solve the Poisson potential equation (1.10) or (1.11). The scheme for the MD-LDG method is similar to (2.3). The major difference is the way to choose the fluxes to fit the Dirichlet boundary conditions and to get minimal dissipation. One way for the fluxes is  $\widehat{u}_h = u_h^-$  and  $\widehat{q}_h = q_h^+$  at the internal cell interfaces,  $\widehat{u}_{h,\frac{1}{2}} = u(a)$ ,  $\widehat{u}_{h,N+\frac{1}{2}} = u(b)$  and  $\widehat{q}_{h,N+\frac{1}{2}} = q_{N+\frac{1}{2}}^- - \alpha(u_{N+\frac{1}{2}}^- - u(b))$  at the boundaries. Another way is to use  $\widehat{u}_h = u_h^+$  and  $\widehat{q}_h = q_h^-$  at the internal cell interfaces,  $\widehat{u}_{h,\frac{1}{2}} = u(a)$ ,  $\widehat{u}_{h,N+\frac{1}{2}} = u(b)$  and  $\widehat{q}_{h,\frac{1}{2}} = q_{\frac{1}{2}}^+ - \alpha(u(a) - u_{\frac{1}{2}}^+)$  at the boundaries, where  $\alpha = O(1/h)$ . In [9], the authors proved optimal convergence for both  $u$  and  $q$  in one dimension, and optimal convergence for  $u$  but suboptimal convergence for  $q$  in two dimensions.

### 2.3 The WKB-LDG Scheme

The WKB-LDG scheme is a WKB scheme based on the LDG method. More precisely, if we consider a “constant form” of the WKB asymptotics, the finite element space for our WKB-LDG method is

$$E^2(\alpha) = \{v_h : (v_h)|_{I_j} \in \text{span}\{1, e^{i\alpha_j(x-x_j)}, e^{-i\alpha_j(x-x_j)}\}, j = 1, \dots, N\}, \tag{2.8}$$

where

$$\alpha_j = \frac{\sqrt{2m}}{\hbar} \sqrt{E + qV(x_j)}, \quad j = 1, \dots, N. \tag{2.9}$$

The approximation space  $E^2(\alpha)$  is actually an exponential space. In [18], the authors have proved the  $L^2$  stability and error estimates of the DG method based on non-polynomial approximation spaces including exponential spaces for time-dependent PDEs. Similar proof

can also be obtained for stationary problems. In particular,  $E^2(\alpha)$  has a third order approximation convergence rate. The proof is simple: we write

$$\begin{pmatrix} 1 \\ e^{i\alpha_j(x-x_j)} \\ e^{-i\alpha_j(x-x_j)} \end{pmatrix} = \begin{pmatrix} 1 & 0 & 0 \\ 1 & i\alpha_j & -\frac{\alpha_j^2}{2} \\ 1 & -i\alpha_j & -\frac{\alpha_j^2}{2} \end{pmatrix} \begin{pmatrix} 1 \\ (x-x_j) \\ (x-x_j)^2 \end{pmatrix} + \begin{pmatrix} 0 \\ -\frac{i\alpha_j^3}{3!} \\ \frac{i\alpha_j^3}{3!} \end{pmatrix} (x-x_j)^3 + O((\Delta x_j)^4).$$

for  $x \in I_j$ , and denote

$$A = \begin{pmatrix} 1 & 0 & 0 \\ 1 & i\alpha_j & -\frac{\alpha_j^2}{2} \\ 1 & -i\alpha_j & -\frac{\alpha_j^2}{2} \end{pmatrix}, \quad b = \begin{pmatrix} 0 \\ -\frac{i\alpha_j^3}{3!} \\ \frac{i\alpha_j^3}{3!} \end{pmatrix}. \tag{2.10}$$

It is easy to verify that  $A$  is invertible and  $A$  and  $b$  are independent of  $\Delta x_j$ . By Proposition 3.1 in [18],  $E^2(\alpha)$  is a third order approximation space. Therefore, even when the solution of the PDE is not close to the asymptotic functions in this approximation space, we should still obtain comparable accuracy as the regular polynomial-based DG method using the same number of degrees of freedom.

As a simple example, we assume  $V$  is constant and solve the simple PDE

$$\begin{cases} -u'' - 4u = 0, & x \in [0, 2\pi], \\ u(0) = 0; & u'(2\pi) = 2. \end{cases} \tag{2.11}$$

The exact solution for this problem is  $u = \sin(2x)$ . The numerical results obtained by the WKB-LDG method using the space  $E^2(\alpha)$  with different values of  $\alpha$ , and the regular polynomial-based DG method, are shown in Table 1. If we choose  $\alpha = 2$  which corresponds to the correct asymptotic value, we can obtain basically the round-off error (in quadruple precision). If, however, we choose a different value for  $\alpha$ , either smaller ( $\alpha = 1$ ), or bigger ( $\alpha = 3$ ), we will not have any advantage over the regular, polynomial-based LDG method, as the exact solution is not closer to  $E^2(\alpha)$  than to  $P^2(I_j)$ . However, even in these cases we

**Table 1**  $L^2$  errors and orders of accuracy for the WKB-LDG method using the space  $E^2(\alpha)$  with different values of  $\alpha$ , and the regular polynomial-based DG method

$N$	$L^2$ error	$L^2$ error	Order	$L^2$ error	Order	$L^2$ error	Order
	$\alpha = 2$	$\alpha = 1$		$\alpha = 3$		LDG $P^2$	
10	4.42E-29	1.31E-2	-	2.38E-2	-	1.73E-2	-
20	6.30E-27	1.61E-3	3.03	2.71E-3	3.14	2.15E-3	3.01
40	1.45E-25	2.01E-4	3.00	3.36E-4	3.01	2.68E-4	3.00
80	1.56E-23	2.51E-5	3.00	4.19E-5	3.00	3.35E-5	3.00
160	1.33E-21	3.14E-6	3.00	5.24E-6	3.00	4.19E-6	3.00

still obtain the expected third order convergence and the error levels for the same mesh are comparable with that of the regular, polynomial-based LDG method.

If we would like to have higher order convergence, we can consider the higher order exponential space

$$E^4(\alpha) = \{v_h : (v_h)|_{I_j} \in \text{span}\{1, e^{i\alpha_j(x-x_j)}, e^{-i\alpha_j(x-x_j)}, e^{i\alpha_j(x-x_j)}(x-x_j), e^{-i\alpha_j(x-x_j)}(x-x_j)\},$$

$$j = 1, \dots, N\}, \tag{2.12}$$

and so on.

*Remark 1* To make sure the basis functions are well defined, it is necessary to require that  $\alpha_j$  is not an integer multiple of  $\pi$ , otherwise the basis functions will be linearly dependent. This is the so-called non-resonance condition (see [4]). Typically, the point  $x_j$  satisfying  $\alpha_j = 0$  (i.e.  $|E + qV(x_j)| = 0$ ) is called a turning point. In this case, we define a threshold  $\delta > 0$ . When  $|E + qV(x_j)| \geq \delta$ , the space  $E^2(\alpha)$  will be used; when  $|E + qV(x_j)| < \delta$ , we simply use  $E^2(\alpha_0)$ , where  $\alpha_0 = \frac{\sqrt{2m}}{\hbar} \sqrt{\delta}$ .

### 3 Numerical Results

In this section, we demonstrate our WKB-LDG method by some numerical simulations of the RTD model. First, we concentrate on the WKB-LDG scheme for the linear Schrödinger equations. By ‘linear’, we mean that we solve the Schrödinger equation (1.1) only without coupling it to the equations for density and self-consistent potential. The energy and total potential are given in advance. Here the total potential is precomputed by a reference solution which is obtained using the regular, polynomial-based LDG  $P^2$  method with 1350 cells. Next, our WKB-LDG scheme is tested on fully non-linear problems. It will couple the integration (1.5) for the density and the Poisson potential equation (1.11) for the self-consistent potential.

In all the numerical simulations, we use the same parameters as those used in [4], see Table 2. As mentioned before, the reference solution is obtained with the regular, polynomial-based LDG  $P^2$  method with 1350 cells.

#### 3.1 The Schrödinger Equation

In this section, we concentrate on the efficiency and accuracy of the WKB-LDG scheme for the linear Schrödinger equation. First, we test our WKB-LDG scheme on a simple case where the exact solutions are available. Next, we will add a non-zero potential bias and consider the self-consistent potential in the simulation, which will introduce turning points.

**Table 2** RTD parameters

$a$	$a_1$	$a_2$	$a_3$	$b_3$	$b_2$	$b_1$	$b$	$m_{eff}$	$V_1$
0 nm	50 nm	60 nm	65 nm	70 nm	75 nm	85 nm	135 nm	$0.067m_e$	$-0.3$ V

**Table 3** Results in the linear case with exact solution

	$N$	$L^2$ error	$N$	$L^2$ error
	$E = 0.0895$ eV		$E = 0.046072$ eV	
WKB-LDG	13	4.63E-14	13	1.57E-16
	23	2.63E-12	23	6.78E-16
LDG $P^1$	135	2.66E-4	135	2.00E-5
	1350	1.76E-6	1350	1.84E-7
LDG $P^2$	135	6.00E-6	135	4.90E-7
	1350	6.13E-9	1350	4.94E-10

### 3.1.1 A Simple Case

If there is no bias applied to the RTD model and we do not consider the self-consistent potential, the total potential  $V$  is piecewise constant and the Schrödinger equation has an analytical solution. Therefore it is easy to use this simple case to test the accuracy of the schemes. We use the same examples as those in [4]. One example has the energy very close to the double-barrier first resonant energy  $E_p^a = 0.0895$  eV and the other has the energy far from this value  $E_p^a = 0.046072$  eV. The total potential  $V = V_e$ ,

$$V_e(x) = \begin{cases} 0, & x < a_2 \\ V_1, & a_2 < x < a_3 \\ 0, & a_3 < x < b_3 \\ V_1, & b_3 < x < b_2 \\ 0, & b_2 < x \end{cases} \tag{3.1}$$

We solve the linear Schrödinger equation (1.1) under these two energies. The errors are listed in Table 3. We list the results of the WKB-LDG scheme with 13 cells and with 23 cells. The mesh with 13 cells contains 2 cells each in  $[a, a_1]$ ,  $[a_1, a_2]$ ,  $[a_2, a_3]$ ,  $[b_3, b_2]$ ,  $[b_2, b_1]$ ,  $[b_1, b]$ , and one cell in  $[a_3, b_3]$ . The mesh with 23 cells contains 6 cells each in  $[a, a_1]$ ,  $[b_1, b]$ , 2 cells each in  $[a_1, a_2]$ ,  $[b_2, b_1]$ ,  $[a_2, a_3]$  and  $[b_3, b_2]$ , and 3 cells in  $[a_3, b_3]$ . We can see that the WKB-LDG method presents only a round-off error in the linear case. As a comparison, the polynomial-based LDG  $P^1$  method has a second order convergence and the LDG  $P^2$  method has a third order convergence. Notice that LDG  $P^2$  with 1350 cells has a comparable accuracy as the WKB-LDG method. That is the reason we choose the LDG  $P^2$  with 1350 cells to produce the reference solution in all the simulations in this paper.

We can also see the perfect match between the WKB-LDG solution and the exact solution from the figures. Figure 1 shows the wave function modulus at the resonant energy  $E_p^a = 0.0895$  eV and Fig. 2 shows the case of a non-resonant energy  $E_p^a = 0.046072$  eV. Both of the figures use a WKB mesh of 13 cells.

### 3.1.2 A Case with Turning Points

We add a bias of 0.08 V at the edges of the device and a precomputed self-consistent potential into the Schrödinger equation (1.1). This time we do not have an analytical solution any more, hence we use a reference solution obtained with the polynomial-based LDG  $P^2$  method of 1350 cells. In the case of turning points, we use a threshold of  $\delta = 0.001$  eV.

We consider 4 different energies, a very low energy  $E = 0.0039$  eV, a low energy  $E = 0.059$  eV, a higher energy  $E = 0.17$  eV and a very high energy  $E = 1.11$  eV. The errors are

**Fig. 1** Comparison among the exact solution, the WKB-LDG solution and the LDG  $P^1$  solution: resonant case with  $E = 0.0895$  eV. 13 cells are used in the WKB-LDG method. 135 cells are used in the LDG  $P^1$  method

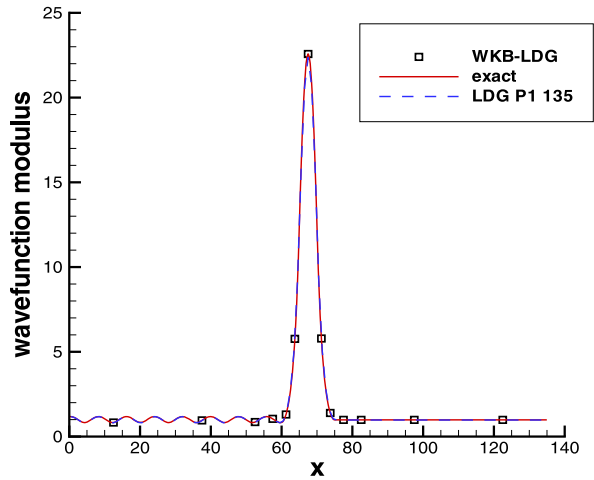
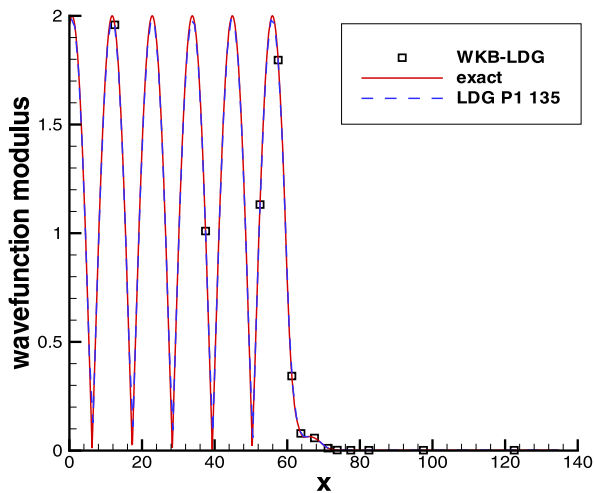


**Fig. 2** Comparison among the exact solution, the WKB-LDG solution and the LDG  $P^1$  solution: non-resonant case with  $E = 0.046072$  eV. 13 cells are used in the WKB-LDG method. 135 cells are used in the LDG  $P^1$  method



listed in Table 4. We only test the WKB-LDG scheme with 23 cells this time. The errors of the WKB-LDG method with 23 cells and the LDG  $P^2$  method with 135 cells have similar magnitude of errors. That is, the WKB-LDG method uses only 17% of the cells used by the LDG  $P^2$  method and much less computational time to reach the same resolution.

We also show the figures of the wave function modulus at the energy  $E = 0.0039$  eV,  $E = 0.059$  eV,  $E = 0.17$  eV and  $E = 1.11$  eV in Figs. 3, 4, 5 and 6 respectively. All of them are using a mesh size of 23 cells. We plot the WKB-LDG solution completely as a function, not just a sample point in each cell, and we can see that the WKB-LDG solution reproduces the reference solution very well.

### 3.2 The Fully Non-linear Problem

In this section, the WKB-LDG scheme is illustrated on the fully non-linear RTD model. The electronic density is computed using (1.5) with an integration between  $-k_{\max}$  and  $k_{\max}$ .

**Table 4** Results in the linear case with turning points

	$N$	$L^2$ error	$N$	$L^2$ error
	$E = 0.0039$ eV		$E = 0.059$ eV	
WKB-LDG	23	1.42E-4	23	2.69E-4
LDG $P^2$	135	2.07E-5	135	1.80E-5
	$E = 0.17$ eV		$E = 1.11$ eV	
WKB-LDG	23	5.96E-5	23	4.56E-5
LDG $P^2$	135	6.92E-6	135	5.23E-5

**Fig. 3** Comparison between the reference solution and the WKB-LDG solution:  $E = 0.0039$  eV. 23 cells are used in the WKB-LDG method. In each cell, the WKB-LDG solution is plotted as a function using 9 points

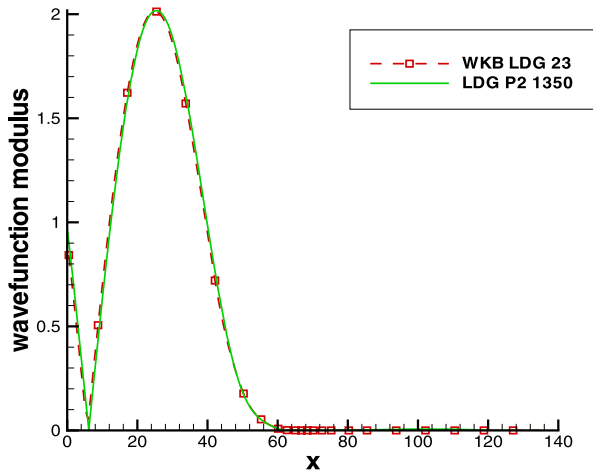
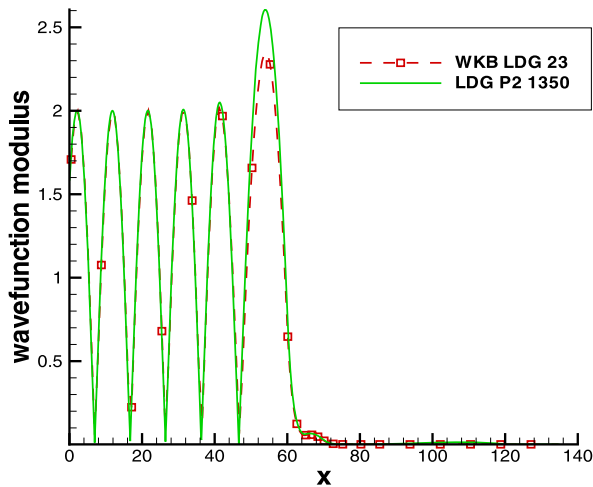


**Fig. 4** Comparison between the reference solution and the WKB-LDG solution:  $E = 0.059$  eV. 23 cells are used in the WKB-LDG method. In each cell, the WKB-LDG solution is plotted as a function using 9 points



where  $k = \sqrt{2mE}/\hbar$  is used instead of the energy  $E$  (see [4]). We use the trapezoidal rule (which is spectrally accurate for compactly supported analytical functions) to evaluate the integral and take a mesh size  $\Delta k$  for the integral. The self-consistent potential is computed

**Fig. 5** Comparison between the reference solution and the WKB-LDG solution:  $E = 0.17$  eV. 23 cells are used in the WKB-LDG method. In each cell, the WKB-LDG solution is plotted as a function using 27 points

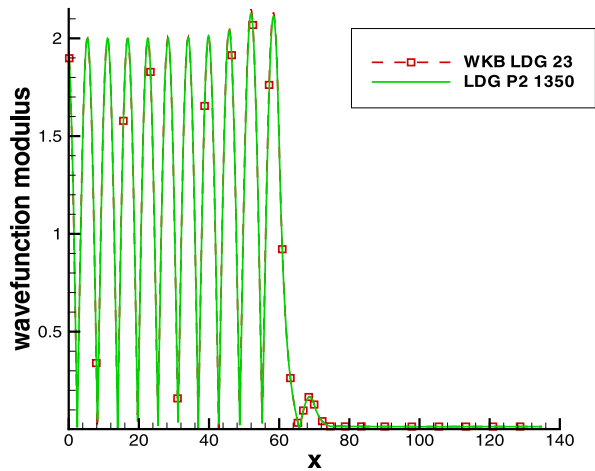


**Fig. 6** Comparison between the reference solution and the WKB-LDG solution:  $E = 1.11$  eV. 23 cells are used in the WKB-LDG method. In each cell, the WKB-LDG solution is plotted as a function using 27 points

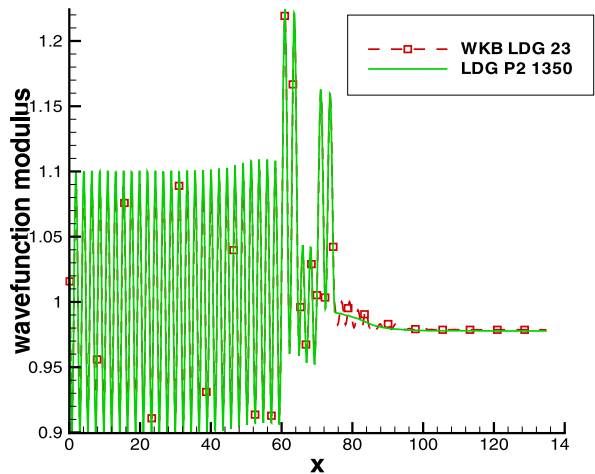


**Table 5** Parameters used for the density and the self-consistent potential computation

$T$	$n_d^1$	$n_d^2$	$k_{\max}$	$\Delta k$	$V_{ref}$	$\epsilon_r$
300 K	$10^{18} \text{ cm}^{-3}$	$10^{15} \text{ cm}^{-3}$	$0.0626 \text{ \AA}^{-1}$	$10^{-3} \text{ \AA}^{-1}$	0.03 V	11.44

using the Gummel iteration described in Sect. 1.1. The parameters we use are listed in Table 5.

We still use the polynomial-based LDG  $P^2$  method with 1350 cells to produce a reference solution and use the same 23 cells for the WKB-LDG method. In [4], it is remarked that a WKB mesh with these few cells might be too coarse for computing the density and the self-consistent potential, and an interpolation could be used to obtain a finer mesh for the purpose of density or self-consistent potential computation. Our numerical results using the WKB-LDG method turn out to be very good if we use the same 23 cells throughout the

**Table 6** Results in the fully non-linear problem: CPU time (seconds/iteration)

	$N$	$L^2$ error bias = 0 eV	CPU time	$L^2$ error bias = 0.08 eV	CPU time
WKB-LDG	23	3.57E-4	2.43	9.72E-4	2.53
LDG $P^2$	135	1.15E-4	10.29	1.15E-4	10.38

**Fig. 7** Comparison between the reference solution and the WKB-LDG solution: density for the fully non-linear case. 23 cells are used in the WKB-LDG method

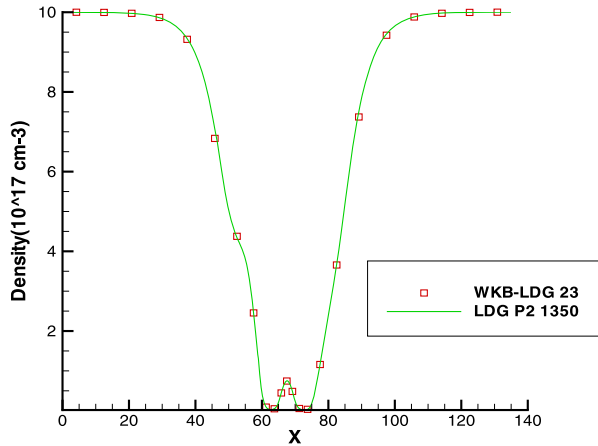
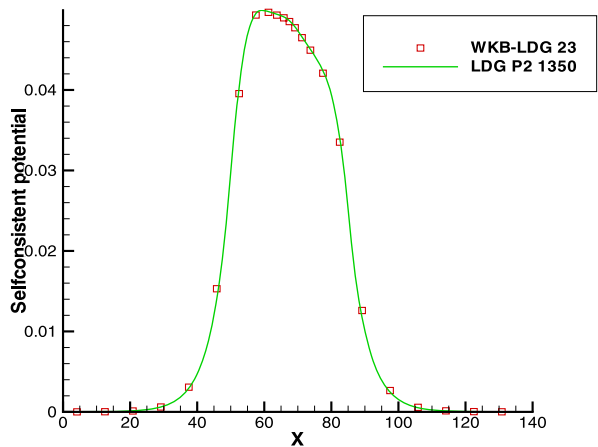


**Fig. 8** Comparison between the reference solution and the WKB-LDG solution: self-consistent potential for the fully non-linear case. 23 cells are used in the WKB-LDG method



simulation. Therefore, we have kept the same mesh for the wave function computation as well as for the computation of the density and the self-consistent potential.

Table 6 lists the errors of the density in both the zero bias case and the 0.08 eV bias case. We can see that the WKB-LDG method gives a pretty good result here. Also it saves around 70% computational time compared to similar results obtained by the regular polynomial-based LDG method.

We present the figures of the density and the self-consistent potential under 0.08 eV bias in Figs. 7 and 8. The WKB-LDG results and the reference solutions overlap very well.

**Fig. 9** Comparison between the reference solution and the WKB-LDG solution: the  $I$ - $V$  characteristics of a resonant tunneling diode. 23 cells are used in the WKB-LDG method

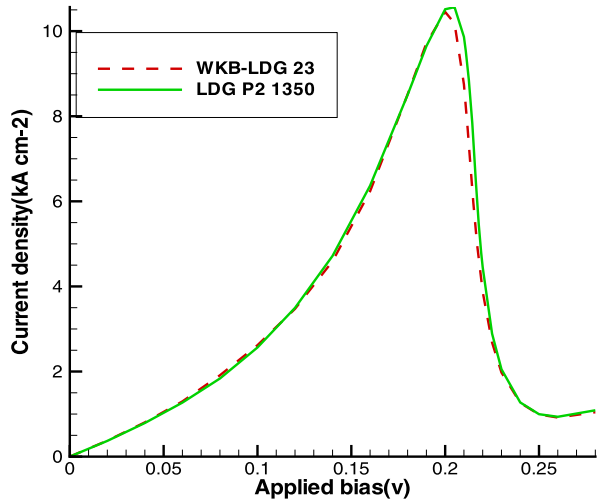
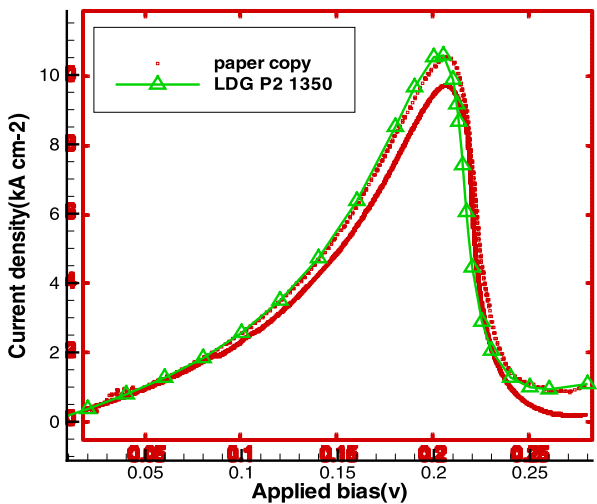


**Fig. 10** Comparison between the reference solution used in this paper and that used in Fig. 20 of [4]: the  $I$ - $V$  characteristics of a resonant tunneling diode. *Solid line with triangle*: the reference solution used in this paper; *dashed line*: the reference solution in Fig. 20 of [4]; *thicker solid line*: the continuous finite element WKB result with 34 points in Fig. 20 of [4]



An important curve, the  $I$ - $V$  curve, is the function of current in (1.8) versus the applied voltage bias. The obtained curve is shown in Fig. 9. The results obtained by the WKB-LDG method with 23 cells are almost indistinguishable from the reference results. For the purpose of verification, we also compare our reference solution with the reference solution reported in Fig. 20 of [4], see Fig. 10. We observe that the two reference solutions overlap well. By comparing Fig. 9 with Fig. 20 of [4], we conclude that our WKB-LDG method with 23 cells produces a solution which is much closer to the reference solution than the continuous finite element WKB result with 34 points.

## 4 Concluding Remarks

In this paper, we have developed a multiscale WKB local discontinuous Galerkin (WKB-LDG) solver for the semiconductor resonant tunneling diode (RTD) model. The main ingredient of this scheme is the WKB-LDG method for solving the Schrödinger equations. Numerical experiments indicate that the WKB-LDG solver has excellent accuracy on very coarse meshes. Compared with the continuous finite element based WKB method in [4], the WKB-LDG method allows the full usage of the potential of this methodology in easy  $h$ - $p$  adaptivity and feasibility for the extension to two-dimensional case. In future work, we will generalize our WKB-LDG method to two-dimensional devices, starting from those with a strong fixed directional dependence such as the double gate MOSFETs in [3], and then moving on to further explore this method to fully two-dimensional problems with changing and eventually no privileged direction.

## References

1. Arnold, D.N., Brezzi, F., Cockburn, B., Marini, L.D.: Unified analysis of discontinuous Galerkin methods for elliptic problems. *SIAM J. Numer. Anal.* **39**, 1749–1779 (2002)
2. Ben Abdallah, N., Degond, P., Markowich, P.A.: On a one-dimensional Schrödinger Poisson scattering model. *Z. Angew. Math. Phys.* **48**, 135–155 (1997)
3. Ben Abdallah, N., Mouis, M., Negulescu, C.: An accelerated algorithm for 2D simulations of the quantum ballistic transport in nanoscale MOSFETs. *J. Comput. Phys.* **225**, 74–99 (2007)
4. Ben Abdallah, N., Pinaud, O.: Multiscale simulation of transport in an open quantum system: Resonances and WKB interpolation. *J. Comput. Phys.* **213**, 288–310 (2006)
5. Ben Abdallah, N., Pinaud, O., Gardner, C.L., Ringhofer, C.: A comparison of resonant tunneling based on Schrödinger's equation and quantum hydrodynamics. *VLSI Des.* **15**, 695–700 (2002)
6. Bohm, D.: *Quantum Theory*. Dover, New York (1989)
7. Chen, Z., Cockburn, B., Gardner, C., Jerome, J.W.: Quantum hydrodynamic simulation of hysteresis in the resonant tunneling diode. *J. Comput. Phys.* **117**, 274–280 (1995)
8. Chen, Z., Cockburn, B., Jerome, J.W., Shu, C.-W.: Mixed-RKDG finite element methods for the 2d hydrodynamic model for semiconductor device simulation. *VLSI Des.* **3**, 145–158 (1995)
9. Cockburn, B., Dong, B.: An analysis of the minimal dissipation local discontinuous Galerkin method for convection-diffusion problems. *J. Sci. Comput.* **32**, 233–262 (2007)
10. Cockburn, B., Shu, C.-W.: Runge-Kutta discontinuous Galerkin methods for convection-dominated problems. *J. Sci. Comput.* **16**, 173–261 (2001)
11. Gummel, H.K.: A self-consistent iterative scheme for one-dimensional steady state transistor calculations. *IEEE Trans. Electron Dev.* **11**, 455–465 (1964)
12. Liu, Y., Shu, C.-W.: Local discontinuous Galerkin methods for moment models in device simulations: Formulation and one-dimensional results. *J. Comput. Electron.* **3**, 263–267 (2004)
13. Liu, Y., Shu, C.-W.: Local discontinuous Galerkin methods for moment models in device simulations: Performance assessment and two-dimensional results. *Appl. Numer. Math.* **57**, 629–645 (2007)
14. Negulescu, C.: Numerical analysis of a multiscale finite element scheme for the resolution of the stationary Schrödinger equation. *Numer. Math.* **108**, 625–652 (2008)
15. Negulescu, C., Ben Abdallah, N., Polizzi, E., Mouis, M.: Simulation schemes in 2D nanoscale MOSFETs: A WKB based method. *J. Comput. Electron.* **3**, 397–400 (2004)
16. Pinaud, O.: Transient simulations of a resonant tunneling diode. *J. Appl. Phys.* **92**, 1987–1994 (2002)
17. Polizzi, E., Ben Abdallah, N.: Subband decomposition approach for the simulation of quantum electron transport in nanostructures. *J. Comput. Phys.* **202**, 150–180 (2005)
18. Yuan, L., Shu, C.-W.: Discontinuous Galerkin method based on non-polynomial approximation spaces. *J. Comput. Phys.* **218**, 295–323 (2006)
19. Yuan, L., Shu, C.-W.: Discontinuous Galerkin method for a class of elliptic multi-scale problems. *Int. J. Numer. Methods Fluids* **56**, 1017–1032 (2008)